ELSEVIER

Materials Science and Engineering A355 (2003) 144–153

MATERIALS SCIENCE & ENGINEERING A

www.elsevier.com/locate/msea

A study of microstructure and microsegregation of aluminum 7050 alloy

Fanyou Xie [a], Xinyan Yan [b], Ling Ding [a], Fan Zhang [c], Shuanglin Chen [c], Men G. Chu [b], Y. Austin Chang [a,*]

[a] *Department of Materials Science and Engineering, University of Wisconsin-Madison, 1509 University Avenue, Madison, WI 53706, USA*
[b] *Alcoa Technical Center, Alcoa Inc., Alcoa Center, PA 15069, USA*
[c] *CompuTherm LLC, 437 S. Yellowstone Dr., Suite 217, Madison, WI 53719, USA*

Received 7 August 2002; received in revised form 9 January 2003

Abstract

An Al 7050 alloy containing 11 components was directionally solidified with two cooling rates of 0.45 and 0.9 K s^{-1}. The microstructure and microsegregation in the solidified alloy were experimentally determined by metallography, scanning electron microscopy, image analysis, X-ray map and EPMA. The microstructures of the alloy solidified with the two cooling rates exhibited dendritic structures. Al, Sigma, S, θ, Mg_2Si, Al_7Cu_2Fe and $Al_{13}Fe_4$ were found in the solidified structure. The volume fractions of solids and solute concentration gradients in the dendrites were studied experimentally by image analysis and an area scan technique, and numerically by using a modified Scheil model, respectively. The model predictions were coupled with robust phase diagram calculation package PANENGINE. The calculated results from the modified Scheil model were in good agreement with the measured data. The PanAluminum–Aluminum Database was used to obtain the needed Gibbs free energies of all phases during the modeling.

Keywords: Al 7050; Microsegregation; Solidification; Experiment; Modeling

1. Introduction

Microstructure and microsegregation are of technical importance for the metal industry, since they are the strategic links between materials processing and materials behavior. For example, the presence of secondary phases formed by Cr, Fe, Mn, Ni, Si and Ti, and combinations thereof during non-equilibrium solidification conditions can increase strength and hardness of aluminum alloys. Variations of concentration may produce inhomogeneous precipitation during subsequent heat treatment thus leading to poor fatigue and corrosion resistance. Therefore an understanding of microstructure and microsegregation is essential for materials development. Numerous experimental and theoretical studies have been carried out to investigate the mechanisms leading to the development of microstructure and microsegregation in binary and ternary systems [1–8]. However, investigations of such behavior for higher order multi-component alloys are rather limited. Since most commercial alloys contain more than 10 components, it is timely to experimentally investigate solidification of multi-component and complex alloys coupled with computation. Lately, a number of simulation studies have been carried out to predict microstructure and microsegregation in higher order systems with microscopic models taking into consideration of some thermodynamic and kinetic effects [9–13]. The state-of-the-art solidification simulation methods have been summarized by Kraft and Chang [14]. However, the microscopic models used for the multi-component alloys were extended from low order systems, especially from binary systems [3,5,6]. More stringent tests are required in applying the microsegregation modeling to commercial alloys with many components. Unfortunately, few experimental investigations have been made to provide sufficient information on microstructure and microsegregation due to the

* Corresponding author. Tel./fax: +1-608-262-0389.
E-mail address: chang@engr.wisc.edu (Y.A. Chang).

0921-5093/03/$ - see front matter
doi:10.1016/S0921-5093(03)00056-X

complexity of increasing numbers of solute elements and phases in multi-component systems such as commercial aluminum alloys.

The objective of present study is to carry out experiments to investigate the microstructure and microsegregation for Al 7050 alloy and compare the analysis to predictions from microscopic modeling. The Al 7050 sample alloy was cast at the Alcoa Technical Center with the composition listed in Table 1. It contains a total of 11 components. The alloy was first directionally solidified, and then its microstructure and microsegregation examined using metallography, scanning electron microscopy (SEM), image analysis, X-ray map and EPMA. The measured experimental data were then compared with simulation results from microscopic modeling. The microscopic model used is a one-dimensional modified Scheil model taking into consideration of back diffusion in the solid, dendrite arm coarsening and the effects of undercooling [5,6,15,16]. The microscopic model was dynamically coupled with a robust phase diagram calculation engine, PANENGINE [17], since the user-friendly and reliable PANENGINE makes it possible to obtain the heavily needed concentrations of the liquid and solid phase at the liquid/solid interface for multi-component alloys. The required Gibbs energies of all phases in the microscopic modeling were obtained from the PanAluminum—a thermodynamic database developed recently at CompuTherm LLC [18] for commercial aluminum alloys.

2. Experimental methods

2.1. Sample preparation

Directional solidification was used in the present study since it is well established, produces uniform microstructures, and allows better control of solidification conditions [10,19]. A high purity Al_2O_3 tube with 3 mm I.D., 4.5 mm O.D. and 350 mm in length was used to load the alloy specimen for the directional solidification. Surface tension of the molten aluminum alloy made it almost impossible to successfully pour the liquid metal into the thin tube. Therefore, vacuum was applied to overcome this problem. As shown in Fig. 1a, the bulk alloy was first placed in a high purity Al_2O_3 crucible, and the crucible was put in a quartz tube with one end closed, and the other end sealed with an O-ring in a water-cooled copper cover. Then an empty thin Al_2O_3 tube was inserted through the center of this copper cover and sealed with a small O-ring. One end of this Al_2O_3 tube was placed near the top of the Al_2O_3 crucible inside the quartz tube, and the other end was connected to a 3-way valve. The quartz tube was finally put in a vertical resistance furnace. Before the furnace was heated up, the quartz tube was evacuated using a mechanical vacuum pump, and kept under positive argon pressure through the 3-way valve. A thermocouple was placed near the crucible containing the bulk alloy. After the bulk alloy was melted completely, the sample Al_2O_3 tube was pushed down into the liquid metal. The vacuum was then applied to raise the liquid metal up into this thin Al_2O_3 tube. Compared with previous sample preparation [20], this whole process is more reliable, and with less effort involved.

2.2. Directional solidification

The directional solidification apparatus used in present study was also used in our previous studies for binary, ternary and quaternary alloys [6–9]. The directional solidification apparatus consisted of a vertical resistance furnace (Fig. 1b) and a high precision position table. The resistance furnace was equipped with three heating zones. This three-zoned furnace provides the capability of maintaining the desired temperature gradient for the directional solidification, since each zone can be controlled separately. A water-cooling jacket was placed at the bottom of this vertical furnace in order to control the unidirectional solidification of the melt. The sample Al_2O_3 tube with the alloy specimen was inserted through the cooling jacket. The position of the tube was fixed by a sample holder with about 25 cm of its length exposing to the hot zone and the remaining 10 cm to the cold zone. The sample holder was firmly attached to the position table. Since the position table was coupled with a micro-step motor and a computer controlled indexer, the movement of the specimen was accurately and smoothly controlled at speeds varying between 0.2 $\mu m\,s^{-1}$ and 40 $cm\,s^{-1}$ within the stationary furnace. The temperature gradient in the furnace was measured to be 4.5 $^{\circ}C\,mm^{-1}$ [10]. Each of the alloy specimens was superheated to about 100 °C above the liquidus temperature for 1 h prior to the start of directional solidification. The samples were solidified for about 10–15 cm with two cooling rates, 0.45 and 0.9 $K\,s^{-1}$. After the solidified alloy reached the desired length, the

Table 1
The actual bulk composition of Al 7050 alloy in present study (in wt.%)

Cu	Mg	Zn	Cr	Fe	Mn	Ni	Si	Ti	Zr	Al
2.60	2.37	6.56	0.03	0.09	0.05	0.01	0.06	0.018	0.10	Bal.

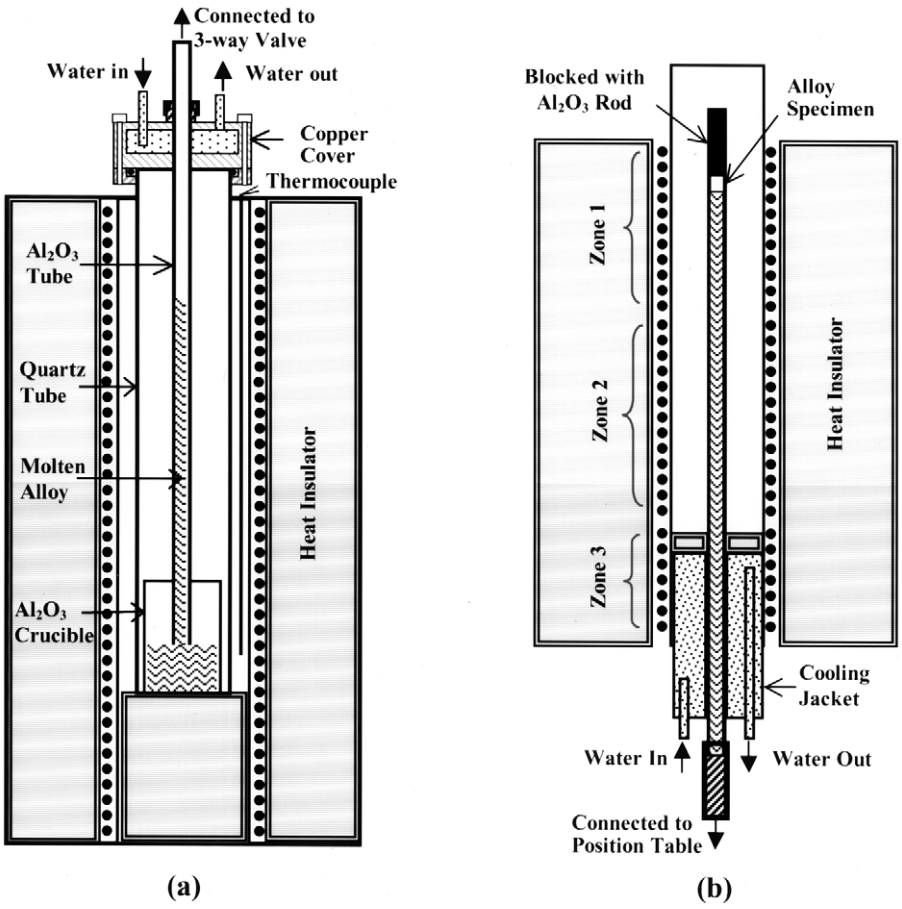

Fig. 1. The schematic drawings of (a) sample preparation furnace, (b) directional solidification apparatus.

specimen was quenched into a water bucket. The solidified sample was subsequently cut in both longitudinal and transverse sections for characterization.

2.3. Sample characterization

The solidified samples were characterized using a CAMECA SX-50 electron microprobe in transverse and longitudinal sections. The operating voltage and the beam current were 15 kV and 20 nA, respectively. The microstructure was examined with optical metallography, SEM, and X-ray maps. The compositions of phases were determined using the wavelength-dispersive spectrometers. The volume fractions of various phases were obtained using a quantitative image analysis program (NIH Image). The EPMA standards used to obtain quantitative composition data were pure elements except MgO for Mg. Following the analysis technique that was employed previously [6,8,9], 441 points were measured automatically over an area of 800×800 μm^2 to determine solute distributions in the area scans. In order to obtain the profile of composition versus volume fraction of solid, measured composition data for a specific solute element were first sorted in ascending order; ordered integer numbers were then assigned to the sorted points and the integer numbers were converted to volume fractions by dividing each data number by the total data number. The normalized value was taken as the fraction of solid, therefore the composition as a function of the fraction of solid can be plotted.

3. Experimental results, solidification modeling and discussion

In this section, the experimental results of microstructure and microsegregation in the aluminum phase are presented and compared them with those obtained by microscopic modeling using a modified Scheil model. The eutectic-like structure and a new sorting method for area scans of multi-component alloy are then discussed.

3.1. Microstructure and microsegregation in the Al phase

The microstructures of Al phase in all solidified samples are dendritic as shown in Fig. 2 for the transverse section and in Fig. 3 for the longitudinal direction. In Figs. 2 and 3 the dark areas are α (aluminum phase) and the bright areas are quaternary Sigma phase, ternary S, or/and binary θ (Al_2Cu phase).

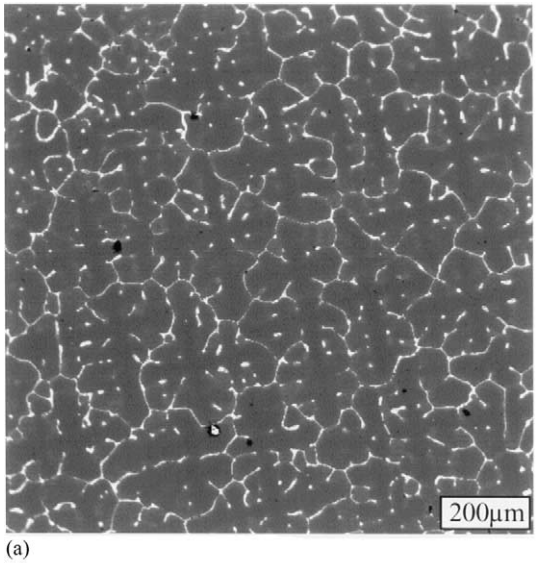

(a)

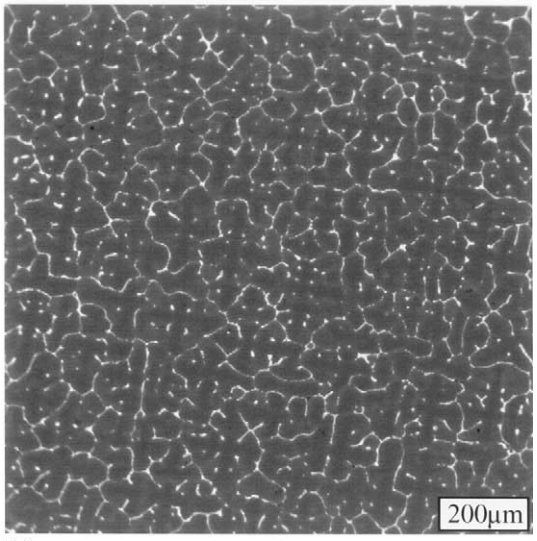

(b)

Fig. 2. Microstructure in transverse sections of Al 7050 alloy solidified with two different cooling rates: (a) 0.45 K s^{-1}; (b) 0.9 K s^{-1} (BSE images).

The Sigma phase here can be described as $(Al,Cu,Zn)_2Mg$, the S phase as Al_2MgCu, and the θ phase as Al_2Cu. The Sigma phase was mainly derived from the binary Zn_2Mg with Cu and Al substituting for Zn at the Zn sublattice [21]. These phases were able to be identified using optical metallogrphy, SEM, X-ray map, and EPMA techniques. As can be seen in Figs. 2 and 3, the dendrite arms are separated by Sigma, S, θ, and/or eutectic-like network, or in touch with each other. The primary stem in Fig. 2 is located at the junction of two secondary arms. The slightly darker gray scales at the center of the dendrites show lower solute contents in the α phase indicating the main growth directions of the dendrite arms. Small isolated intradendritic droplets are also visible especially near the

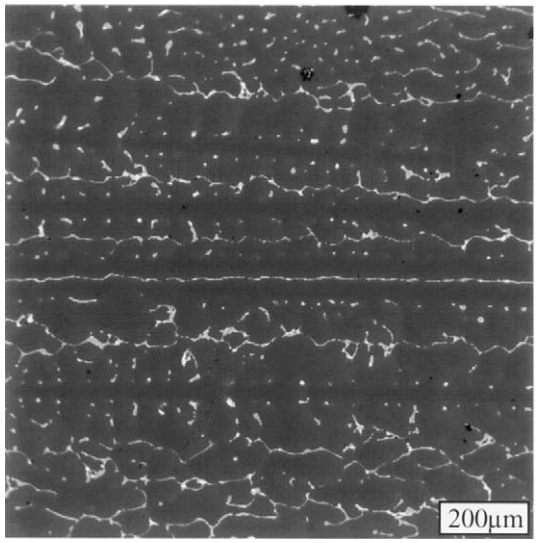

Fig. 3. Microstructure in longitudinal section of Al 7050 alloy solidified with cooling rate of 0.45 K s^{-1} (BSE images).

primary stem and the root of the tertiary arms. The dendritic microstructures are similar to those observed in previous studies [6,9].

The amounts of phases present in the solidified structures were measured with image analysis (NIH), and listed in Table 3 for the fraction of α after solidification. The back scatter electron (BSE) images covering the entire area of the transverse section were used to obtain phase fractions. For cooling rates in present study, the measured solid fraction of α was 94.4 vol.% as given in Table 3. The measured α includes both primary and some secondary α, since secondary α from the subsequent solidification reactions crystallizes on the surfaces of the dendrites and becomes experimentally indistinguishable. The standard deviations of the experimental measurements for the amount of α were less than $\pm 0.3\%$. It was difficult to accurately measure the fraction of each secondary phase such as Sigma, S or θ due to the complex eutectic structure shown in the BSE images.

The area scan method was used to obtain solute redistributions in the solidified structures. Fig. 4 shows the re-distributions of three major solute elements, Cu, Mg and Zn, for this multi-component Al 7050 alloy solidified with a cooling rate of 0.45 K s^{-1}. The measured points originally collected from the area scans were sorted according to the copper composition, since the major phases such as Al, Sigma, S and θ presented in the solidified structure can be clearly distinguished with the content of copper. As will be discussed later, the compositions of Mg and Zn associated with that of Cu were directly plotted in Fig. 4, instead of being sorted independently before plotting. Note that there are local maximum and minimum close to the end of solidification for the Mg concentration profile. This is because of

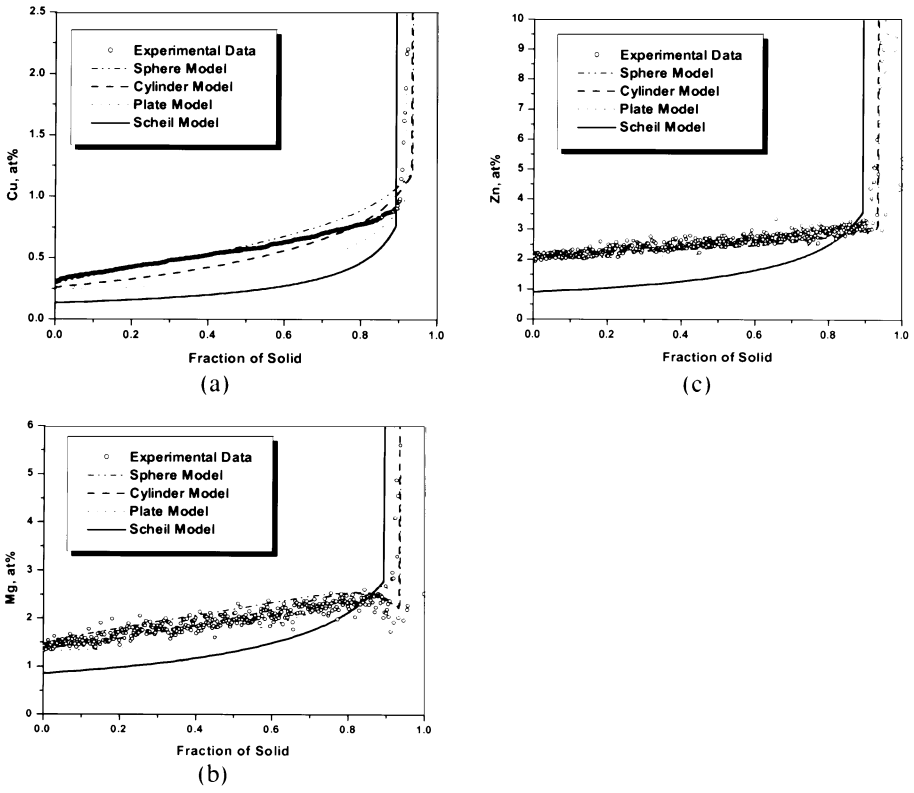

Fig. 4. Measured and calculated concentration profiles of (a) Cu, (b) Mg and (c) Zn for the Al 7050 alloy solidified with a cooling rate of 0.45 K s^{-1}.

the formation of Sigma and S phases during the solidification reaction. Similar results were found for the alloy solidified at 0.9 K s^{-1}, except the solute concentrations of Cu, Mg and Zn at 0.9 K s^{-1} were slightly lower than those at 0.45 K s^{-1} due to the effect of back diffusion in the solid.

In addition to yielding solute re-distribution data, it is also possible to obtain the volume fractions of the α phase formed using the area scan measurements. As can be seen in Fig. 4, the normalized fraction at which the measured Cu concentration suddenly changes corresponds to the total fractions of the α phase formed. This is due to the fact that the Cu composition changes abruptly when the major secondary phase Sigma started to form. As shown in Table 3, the fraction of the α phase determined in this manner is in reasonable agreement with that obtained by image analysis, further supporting the reliability of the data obtained in the present study.

3.2. Microscopic modeling

The model used to calculate the degree of microsegregation was a one-dimensional modified Scheil model incorporating back diffusion in the solid, dendrite arm coarsening and dendrite tip undercooling [5,6,8,15,16]. The main thermodynamic and kinetic effects that may influence the solidification behavior were accounted for. The model calculates the secondary dendrite arm spacing, solute re-distribution in the dendrite arms and types and amounts of non-equilibrium phases in the entire range of solidification for multi-component alloys. Since solidification modeling relies on the phase diagram information, especially the concentrations of the liquid and solid phase (also known as partition coefficients) at the liquid/solid interface, the best approach is to couple microscopic modeling directly with a robust tool of phase diagram calculation for multi-component alloys [6–11,22–25]. PANENGINE, a multi-component phase diagram computation package developed by CompuTherm LLC [17], is used in the present study. The needed Gibbs free energies of phases were obtained from a thermodynamic database, PanAluminum [18]. The PanAluminum was also developed by CompuTherm LLC for the commercial aluminum alloys. It contains 14 elements (Al, Cr, Cu, Fe, Hf, Mg, Mn, Ni, Si, Sr, Ti, V, Zn, and Zr). In addtion to binary and ternary systems, three most important quaternary systems, Al–Cu–Mg–Zn, Al–Cu–Mg–Si and Al–Fe–Mg–Si, were thermodynamically modeled in details for this database [13,21,26]. Moreover, this database was tested with 38 commercial Al-base alloys [18,27,28].

By using the PANENGINE and the aluminum database, tie lines in a multi-component system can be calculated at each time step of the solidification process. Back diffusion in the solid was obtained independently for

each solute element by solving the Fick's second law numerically at each time step. Dendrite arm coarsening was calculated using the model of Roósz et al. [29] with the modified coarsening parameter suggested by Beaverstock [30]. The modified coarsening parameter takes into consideration of all solute elements for a multi-component system instead of only the control solute element with the lowest value of coarsening parameter. The needed physical property data such as diffusion coefficient, surface tension, and latent heat are given in Table 2.

Three geometric shapes, i.e. plate, cylinder and sphere, were used in the modified Scheil model to describe the growing secondary or tertiary arms. The calculated concentration profiles including basic and modified Scheil models were shown in Fig. 4 for the three major solute elements of Cu, Mg and Zn. As can be seen in Fig. 4, the calculated results from the Scheil condition are not satisfactory since they are too low overall compared with the experiments, while the modified Scheil model is more promising. For Cu, the dendrite arm is better described with cylinder geometry only at high fraction of solid, and with sphere at the low end. Cylinder shape worked better for Mg, while both cylinder and sphere worked for Zn.

The phases formed during the solidification can also be predicted with the microscopic modeling. Fig. 5 shows the calculated phase fractions as a function of temperature for the Al 7050 alloy solidified with the cooling rate of 0.45 K s^{-1}. As can be seen in Fig. 5, the calculated phase sequence for the alloy studied was Al, $Al_{13}Fe_4$, Al_3Ni, Al_7Cu_2Fe, Mg_2Si, Sigma, S and θ. Note that the calculated phase fractions of $Al_{13}Fe_4$, Al_3Ni, Al_7Cu_2Fe, Mg_2Si and θ were in the order of 10^{-3} as shown in Fig. 5. Therefore these phases would be very difficult to be detected quantitatively in practice. This evidence was fully supported by the experimental examinations. The calculated phase fraction of α was 94.8%, which was in good agreement with that from the image analysis as listed in Table 3. Table 3 also lists the calculated and measured dendrite arm spacings, and they were in very good agreement as well.

Table 2
Physical data used for Al 7050 alloy in the model calculations

Liquid diffusion coefficient of Cu ($m^2\ s^{-1}$)	$D_L^{Cu} = 1.05 \times 10^{-7} \exp(-2856/T)$	[29]
Solid diffusion coefficient of Cu ($m^2\ s^{-1}$)	$D_S^{Cu} = 4.8 \times 10^{-5} \exp(-16069/T)$	[31]
Liquid diffusion coefficient of Mg ($m^2\ s^{-1}$)	$D_L^{Mg} = 9.90 \times 10^{-5} \exp(-8610/T)$	[32]
Solid diffusion coefficient of Mg ($m^2\ s^{-1}$)	$D_S^{Mg} = 6.23 \times 10^{-6} \exp(-13831/T)$	[33]
Liquid diffusion coefficient of Zn ($m^2\ s^{-1}$)	$D_L^{Zn} = 2.3 \times 10^{-7} \exp(-4162/T)$	[34]
Solid diffusion coefficient of Zn ($m^2\ s^{-1}$)	$D_S^{Zn} = 2.45 \times 10^{-5} \exp(-14385/T)$	[35]
Energy of solid/liquid interface ($J\ m^{-2}$)	$\gamma = 0.093$	[29]
Specific latent heat of solidification ($J\ m^{-3}$)	$\Delta h = 9.5 \times 10^8$	[36]
Geometric factor for coarsening	$G = 35$	[29]

3.3. Eutectic-like structure

The eutectic-like structure in the solidified samples was very complicated, since this Al 7050 alloy consists of 11 components and many phases could participate in the solidification reactions. Let us use the specimen solidified with cooling rate of 0.45 K s^{-1} as an example. Fig. 6 shows the formation of the eutectic-like structure in the network and isolated droplets in a BSE image. It was found that the brightest phase in the BSE images was θ as shown in Fig. 6. The second brightest area was Sigma or S alone, or their mixture since these two phases have similar brightness in the BSE image. Also note that Mg_2Si phase was found in the solidified structure. In order to further identify the Sigma and S phases, and other phases presented in the eutectic mixture structure, the X-ray map technique was applied. Fig. 7 shows the X-ray maps of Cu Kα, Mg Kα, and Fe Kα characteristic lines (labeled at the top left corner of each figure) for the area A in Fig. 6. The intensities of these X-ray maps were normalized individually with the supporting software installed in the CAMECA SX-50 electron microprobe instrument. The Sigma and S phases can be distinguished with the X-ray map of Mg Kα, since the k-ratio (effective X-ray intensity) of Mg in Sigma phase is about 0.054 after the ZAF correction, while the k-ratio of it in S phase is 0.091. In other words, the S phase (at 15 kV) will be about 'twice as intense' as the Sigma phase in the X-ray map of Mg Kα as shown in Fig. 7. The θ phase can be identified with X-ray maps of Cu Kα and Mg Kα. As can be seen in Fig. 7, the θ was located at the area with highest X-ray counts of Cu Kα and lowest X-ray counts of Mg Kα. By using the X-ray maps shown in Fig. 7, it was also found a ternary Al–Cu–Fe phase in the eutectic-like structure. The composition measured by EPMA for this phase was close to Al_7Cu_2Fe.

As mentioned above, the $Al_{13}Fe_4$ phase was predicted in the model calculation, but it was not clearly observed in the solidified structure of Al 7050 alloy. However, the $Al_{13}Fe_4$ phase has been found frequently to be one of the major secondary phases in many commercial Al alloys, especially in the 7xxx series such as 7005 and 7075 [28] with Fe content in the range of 0.2–0.3 wt.%. In order to confirm the existence of $Al_{13}Fe_4$ phase, an Al 7050 sample was wrapped in a carbon paper, heated up above its melting temperature for completely melting, maintained at 580 °C for an hour to stabilize the $Al_{13}Fe_4$ phase (Fig. 5), and then rapidly quenched into a bucket of ice water. The quenched sample was cross-sectioned, polished, and examined using SEM and X-ray

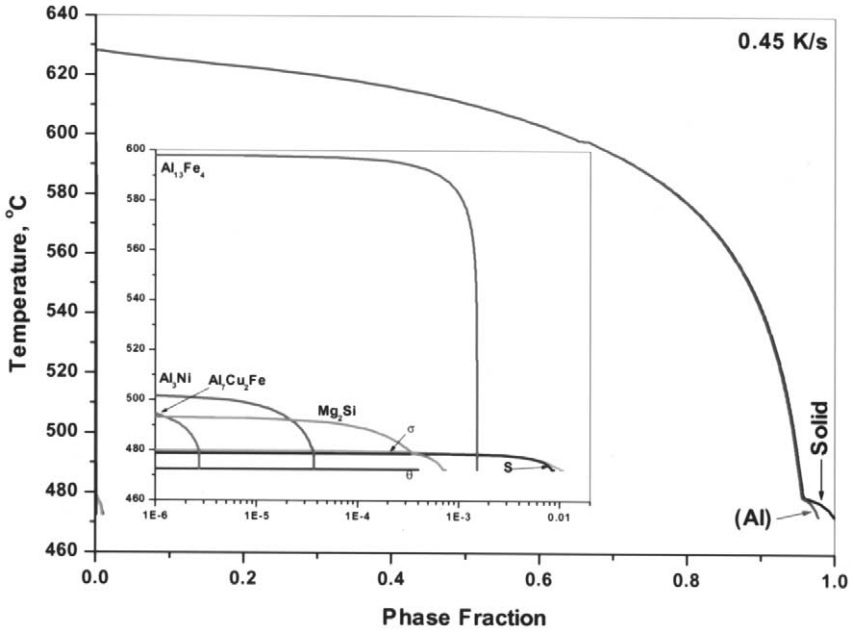

Fig. 5. Model-calculated phase fractions as a function of temperature for the Al 7050 alloy solidified with cooling rate of 0.45 K s^{-1}.

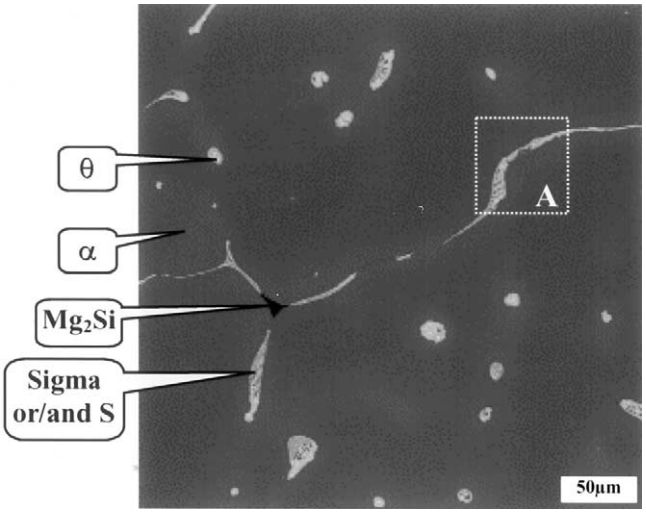

Fig. 6. The eutectic-like structure in the network and isolated droplet (BSE image).

map. A large area covering eutectic-like structure was roughly mapped over with Fe Kα X-ray to identify the spots with high Fe content. Then the spot with highest Fe content was selected for further examination. Fig. 8 shows the X-ray maps as well as the eutectic-like structure in BSE image. As shown in Fig. 8, the divorced eutectic structure contained mostly the Sigma phase with high Cu, Mg, and Zn contents. However, a small part of this area was found to have higher Fe content as shown in the X-ray map of Fe Kα in Fig. 8. This small area was fully embedded in the Sigma phase. Moreover, a tiny bright spot in this Fe Kα map was found to be a phase without Cu, Mg and Zn as shown in the X-ray maps of Cu, Mg, and Zn Kα. Due to the small size and the heterogeneity of the complex eutectic-like structure, it was very difficult to obtain the accurate composition of this tiny spot using EPMA. With the combination of the solidified structure in Fig. 8, the calculated results shown in Fig. 5 and the results suggested by Backerud et al. [28] for other Al 7xxx alloys, it is reasonable to conclude that this tiny spot and the rest of the bright area in the Fe Kα map of Fig. 8 are the mixture of $Al_{13}Fe_4$ and Al_7Cu_2Fe phases. Based on the observation of the quenched sample above, the $Al_{13}Fe_4$ phase will be mixed with the Al_7Cu_2Fe phase in the directional solidification samples as well. Note that the X-ray map of Si Kα was also shown in Fig. 8, since Si is one of the crucial impurities in the commercial aluminum alloys. It was found that there are no other phases,

Table 3
Comparison of experimental and calculated phase fractions and dendrite arm spacings

Cooling rate (K s^{-1})	Amount of Al Phase (vol.%)					λ_2 (μm)	
	Area scan	Image analysis	Modified Scheil	Scheil	Lever rule	Image analysis	Modified Scheil
0.45	92.5	94.4	94.8	89.0	98.3	56	55.2

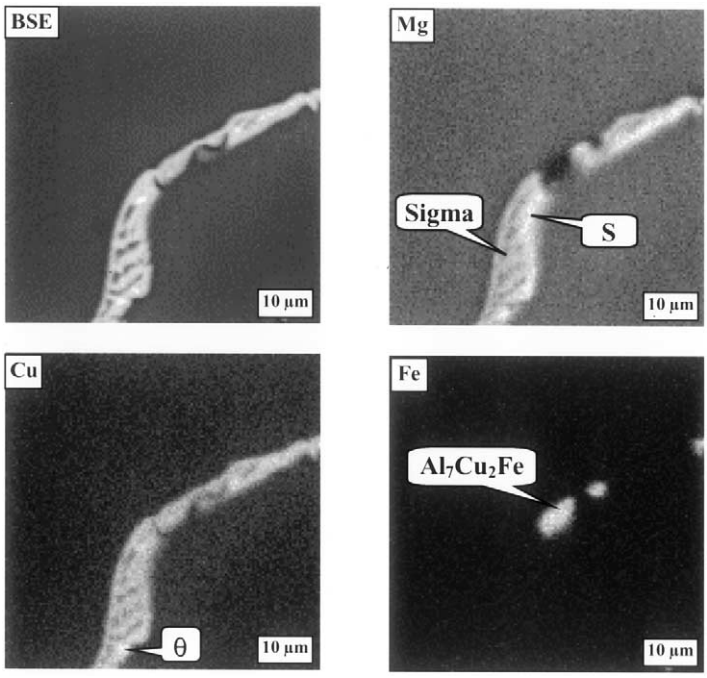

Fig. 7. The X-ray maps of Cu Kα, Mg Kα, and Fe Kα characteristic lines for area *A* in Fig. 6.

except Mg_2Si (Fig. 6), associated significantly with Si through out the examinations.

3.4. New data sorting in the area scan method

The area scan over a large section with many measuring points has been proven to be a very effective method for obtaining solute distributions in the solidified structure [6]. However, it requires that the composition for a particular component in all presented phases is distinguishable. For the Al 7050 alloy solidified with the cooling rates of 0.45 and 0.9 K s^{-1} in present study, the major phases such as Al, Sigma, *S* and *θ* can be separated with the content of copper, therefore the copper composition was used to sort the data points collected from the area scan. In previous studies [6,8,9], each solute composition measured from the area scan was sorted independently; this leads the concentration profile for each element continuously increasing (or decreasing) from the beginning to the end of the solidification. Moreover, this makes comparison with the calculated solute re-distribution difficult if there is a maximum or/and minimum value between the two ends of the calculated concentration profile. Unfortunately, this kind of composition profile with local maximum and/or minimum is often found in a complex multi-component alloys, since the solubilities of solutes in the matrix change during the solidification reactions. For the Al 7050 alloy studied in present work, the calculated concentration profiles of Mg, Fe, Mn and Si all fall in

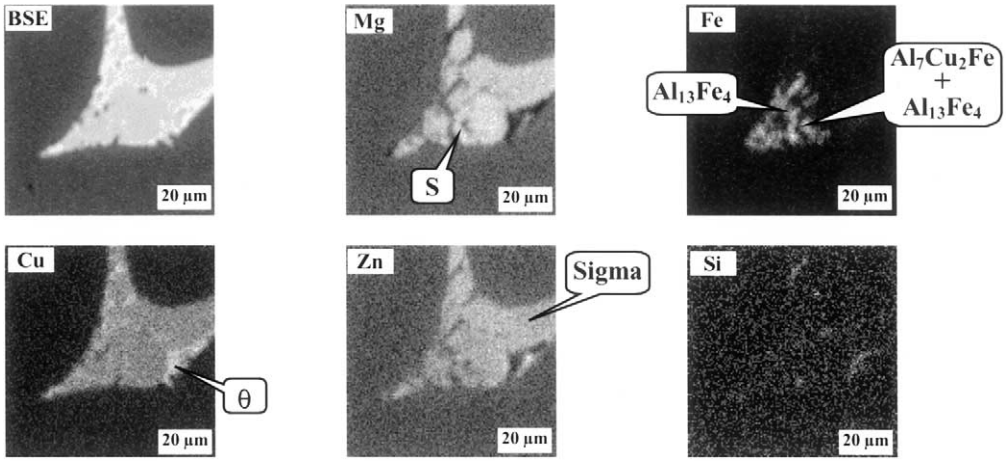

Fig. 8. The X-ray maps of an eutectic area in the Al 7050 alloy quenched from 580 °C.

this category. A new approach has been used for the treatment of area scan data since the solute element of Mg can not be simply neglected in the Al 7050 alloy studied. In this new approach, only the Cu contents of the measuring points were sorted for each area scan, the other solute contents such as Mg and Zn associated with the sorted Cu content at each point were then directly plotted as shown in Fig. 4. The measured Mg concentration profile shown in Fig. 4b includes a local maximum point and a local minimum point around the fraction of solid of 0.94, agrees closely with the calculations from the modified Scheil model.

4. Conclusion

The microstructures and microsegregation of a directional solidified Al 7050 alloy were studied with two cooling rates of 0.45 and 0.9 $K\,s^{-1}$. Metallography, SEM, image analysis, X-ray map and EPMA were used as characterization techniques. The microstructures of the alloy solidified with these two cooling rates exhibited dendritic structures at both transverse and longitudinal sections. The Al, Sigma, S, θ, Mg_2Si, Al_7Cu_2Fe and $Al_{13}Fe_4$ phases were identified in the complex solidified structure. The calculated volume fraction of Al phase was 94.8% and in close agreement with the fraction of Al phase of 94.4% measured by image analysis in the directionally solidified samples.

The microscopic modeling was coupled with a robust phase diagram calculation program, PANENGINE. The needed thermodynamic descriptions of phases were provided by PanAluminum. By using the PANENGINE and PanAluminum, the actual phase diagram data throughout the whole solidification were obtained in the modeling for this Al 7050 alloy containing 11 elements. When the modified Scheil model was used, the calculated phases formed during the solidification, phase fractions, concentration profiles, as well as dendrite arm spacings were in good agreement with those measured by experiment. The basic Scheil condition was not satisfactory for this multi-component alloy studied. It was also found that the dendrite arm was better described with sphere and cylinder rather than plate for the cooling rates studied.

A new sorting method for the area scan technique was introduced to overcome the problems found in the sorted concentration profiles in the previous studies. Only the Cu contents were sorted, and the other solute contents associated with the Cu contents were then directly plotted. The local maximum and minimum determined by area scan for the Mg profile agreed very well with that calculated from modified Scheil model.

Acknowledgements

We wish to thank the National Science Foundation for financial support through grant No. NSF-DMR-94-21780, and Dr Bruce MacDonald of the Metal Program of the Materials and Processing Cluster of NSF for his interest. We also wish to thank the Air Force Laboratory, Dayton, OH, for the partial financial support through SBIR project (Nos. F33651-97-C-5257 and F33615-00-C5514) awarded to CompuTherm, LLC, Madison, WI 53719.

References

[1] T.F. Bower, H.D. Brody, M.C. Flemings, Trans. AIME 236 (1966) 624.
[2] R. Mehrabian, M.C. Flemings, Metall. Trans. 1 (1970) 455.
[3] A. Roósz, H.E. Exner, Acta Metall. Mater. 38 (1990) 375.
[4] J. Lacaze, G. Lesoult, ISIJ Int. 35 (1995) 658.
[5] T. Kraft, M. Rettenmayr, H.E. Exner, Model. Simul. Mater. Sci. Eng. 4 (1996) 161.
[6] F.-Y. Xie, T. Kraft, Y. Zuo, C.-H. Moon, Y.A. Chang, Acta Mater. 47 (1999) 489.
[7] X.-Y. Yan, F.-Y. Xie, M. Chu, Y.A. Chang, Mater. Sci. Eng. A 300 (2001) 268.
[8] X.-Y. Yan, S.-L. Chen, F.-Y. Xie, Y.A. Chang, Acta Materialia 50 (2002) 2199.
[9] F.-Y. Xie, T. Kraft, M. Chu, Y.A. Chang, in: J.L. Anjier (Ed.), Light Metals, TMS, Warrendale, PA, 2001, p. 1085.
[10] F.-Y. Xie, Ph.D. Thesis, University of Wisconsin-Madison, 1999.
[11] D.K. Banerjee, M.T. Samonds, U.R. Kattner, W.J. Boettinger, in: J. Beech, H. Jones (Eds.), Solidification Processing, Dept. Engr. Mater., University of Sheffield, Sheffield, UK, 1997, p. 351.
[12] X.-Y. Yan, et al., J. Alloy Compounds 320 (2001) 151.
[13] X.-Y. Yan, Ph.D. Thesis, University of Wisconsin-Madison, 2001.
[14] T. Kraft, Y.A. Chang, JOM 49 (12) (1997) 20.
[15] G.M. Gulliver, J. Inst. Met. 9 (1913) 120.
[16] E. Scheil, Z. Metallkd. 34 (1941) 70.
[17] PANENGINE 1.1—Phase Diagram Calculation Engine for Multi-component Systems, CompuTherm LLC, Madison, WI53719, 2001.
[18] PanAluminium—Thermodynamic database for Commercial Aluminium Alloys, CompuTherm LLC, Madison, WI53719, 2001.
[19] R.M. Sharp, A. Hellawell, J. Cryst. Growth 5 (1969) 155.
[20] Y. Zuo, Ph.D. Thesis, University of Wisconsin-Madison, 1997.
[21] H. Liang, Ph.D. Thesis, University of Wisconsin-Madison, 1998.
[22] S.-W. Chen, Y.A. Chang, Metall. Trans. 23A (1992) 1038–1043.
[23] Y. Zuo, Y.A. Chang, in: S.K. Das (Ed.), Light Metals, TMS, Warrendale, PA, 1993, p. 935.
[24] B. Sundman, J. Agren, MRS Bull. (USA) 24 (4) (1999) 32.
[25] M. Hillert, L. Hoglund, M. Schalin, Mater. Trans. JIM 41 (8) (2000) 1098.
[26] S. Daniel, Ph.D. Thesis, University of Wisconsin-Madison, 2001.
[27] W.J. Whealon, Ph.D. Thesis, University of Wisconsin-Madison, 1993.

[28] L. Backerud, G. Chai, J. Tamminen, Solidification Characteristics of Aluminum Alloys 1 (1990) 137.
[29] A. Roósz, E. Halder, H.E. Exner, Mater. Sci. Tech. 2 (1986) 1149.
[30] R.C. Beaverstock, in: J. Beech, H. Jones (Eds.), Solidification Processing, Dept. Engr. Mater., University of Sheffield, Sheffield, UK, 1997, p. 321.
[31] D. Bergner, Neue Hütte 29 (1984) 207.
[32] K. Kovacova, D. Grman, Kovove Mater. 17 (1979) 144.
[33] E.A. Brandes, G.B. Brook (Eds.), Smithells Metals Reference Book, seventh ed., Buttetworth Heinemann Ltd, Linacre, Jordan Hill, Oxford OX2 8DP, London, 1992.
[34] B. Wei, D.M. Herlach, B. Feuerbacher, F. Sommer, Acta Metall. Mater. 41 (1993) 1801.
[35] D.L. Beke, T. Godeny, F.J. Kedves, G. Groma, Acta Metall. 25 (1977) 539.
[36] W. Kurz, D.J. Fischer, Fundamentals of Solidification, Trans Tech Pub, Adermannsdorf, Switzerland, 1989.